Cell Reports, Volume *20*

Supplemental Information

Local Nucleation of Microtubule Bundles through Tubulin Concentration into a Condensed Tau Phase

Amayra Hernández-Vega, Marcus Braun, Lara Scharrel, Marcus Jahnel, Susanne Wegmann, Bradley T. Hyman, Simon Alberti, Stefan Diez, and Anthony A. Hyman

SUPPLEMENTAL INFORMATION

Inventory of Supplemental Information

- Supplemental experimental procedures.
- Figures S1-S7.
- Supplemental References.

SUPPLEMENTAL EXPERIMENTAL PROCEDURES

Prediction of tau protein disorder distribution and low complexity domains

To predict the disorder degree along human tau protein (splice variant htau441) PONDR program was employed (http://www.disprot.org/index.php). PONDR-FIT (P-FIT) and VL3 algorithms are shown. These algorithms are generally used to predict the disorder tendency of proteins that are experimentally known to be disordered (Obradovic et al., 2003; Xue et al., 2010). The low complexity domains in htau411 were predicted with SEG program (http://mendel.imp.ac.at/METHODS/seg.server.html, Wootton, 1994). LCD1 region comprises amino acids 129 to 153 and LCD2 amino acids 172 to 223. The level of stringency used was SEG 12 2.2 2.5.

Prediction of proteins net charge distribution

CIDER resource (Classification of Intrinsically Disordered Ensemble) was used to plot the net charge per residue [NCPR, http://pappulab.wustl.edu/CIDER/analysis/, (Holehouse et al., 2015)] for different MAPs and intermediated filaments in figure S7.

Constructs

The cDNA encoding for htau441 (also named 2N4R) was a gift from Peter Klein [tau/pET29b, Addgene plasmid number # 16316, (Hedgepeth et al., 1997)]. Htau441 cDNA was amplified by PCR from this vector using the primers shown in Table S1 and cloned into a baculoviral expression vector (pOCC series). Details of the constructs used are listed in Table S1.
His tag cleaved version of htau441-EGFP-PS-6xhis and htau441-mCherry-PS-6xhis were used in this study. Untagged version of tau (C-terminal 6xhis cleaved) and N-terminal EGFP tagged version of tau were also purified as controls (htau441-PS-6xhis and 6xhis-PS-EGFP-htau441) to assess its capability to form drops and bundles. In both cases drops and bundles were formed. A linker was always present between tau and the fluorescent tag. All constructs generated were confirmed by digestion and sequencing. PS refers to PreScission protease recognizing sequence.

Recombinant proteins expression and purification

Tau variants

All tau variants were purified from insect cells using the baculovirus expression system. Recombinant baculovirus for each construct were produced according to Woodruff and Hyman (2015). Sf9 insect cells (log phase, 1 million cells/ml, Expression system, Cat#94-001F) were infected with 5 ml of P2 baculovirus stock, incubated at 27°C with moderate shaking and harvested 72 hours post infection. Cells were harvested by centrifugation at 700g for 8 min and resuspended in resuspension buffer [25 mM HEPES, 150mM KCl, 20 mM imidazole (pH 7.4) with 1 mM DTT, 1 mM PMSF (Sigma) and 1x Protease inhibitors cocktail (Calbiochem, Type III)]. Cells were lysate using an Emulsiflex (Emulsiflex-C5, Avestin). The cell lysate was spin at 35000 rpm for 45 minutes and the supernatant was collected. The lysate was filtered through a 0.45 µm filter and incubated with Ni-NTA agarose resin (QIAGEN) HiTrap for 1 hour. Disposable gravity columns (20 mL, Biorad) were used to collect and wash the beads. Columns were washed 4 times with 20 ml of wash buffer (25 mM HEPES, 150 mM KCl, 30 mM imidazole, 1 mM DTT, pH 7.4) and eluted with elution buffer (same buffer with 250 mM imidazole). 6xhis tag was removed by treatment with PreScission protease (3C HRV protease, 1:100, 1µg enzyme/100 µg of protein, overnight at 4°C). Imidazole was removed by dialysis (slide-a-lyzer with 20 KDa cut off, overnight at 4°C). His tag cleave was performed simultaneously with the dialysis. The protein was further purified by size-exclusion chromatography using a HiLoad 16/60 Superdex 200 column with and ÄKTA Pure chromatography system (GE Healthcare) in 25 mM HEPES, 150 mM KCl, 1 mM DTT (pH 7.4). Collected peak fractions were concentrated to 100 µM or 200 µM using Amicon Ultra 30K (Millipore). Protein concentration was measured with a NanoDrop ND-1000 spectrophotometer (Thermo Scientific) at 280 nm absorbance. Proteins were flash-frozen in liquid nitrogen and stored at -80°C. All steps in the purification were

performed at 4°C. Purified proteins are shown in figure S1.

Tubulin

Tubulin was purified from porcine brains as previously described (Gell et al., 2011). Purified tubulin (α/β dimers) used is shown in figure S1. Cycled tubulin was dimly labelled with rhodamine or Cy5 fluorescent dyes as previously described and mixed with unlabelled tubulin at a molar ratio of 1:3 (Hyman et al., 1991).

***In vitro* assays**

Droplets fusion with optical tweezer

Controlled drop fusion experiments were conducted in a custom-built dual trap optical tweezer microscope with two movable traps (Jahnel et al., 2011; Patel et al., 2015). Tau droplets were formed with 25 µM tau-EGFP in 25 mM HEPES, 150 mM KCl (pH 7.4) with 10% dextran and 1 mM fresh DTT. 5 µl of this mix were placed in a static flow chamber (coverslip – double-sided tape – coverslip sandwich). Droplets could be trapped at minimal laser intensity (laser power at focal position < 50 mW to prevent heating artifacts) due to a mismatch in the index of refraction between the droplets and the surrounding media. Keeping one optical trap (T1) stationary, the other optical trap was moved until droplets were brought into contact, after which droplet fusion was recorded with 1 ms temporal resolution (1 kHz). The combined laser signal showed two characteristic phases: a fast rise potentially driven by surface tension, and a slower relaxation, governed by viscosity. To quantify the dynamics of tau droplet fusion we describe the process phenomenologically as a two-state exponential relaxation process with the following formula for the laser signal f(t) (magenta fit to time series in Fig. 1c):

$$f(t) = \begin{cases} f_0, & t < T_{\text{off}} \\ f_0 + \alpha(1 - exp(-\frac{t-T_{\text{off}}}{\tau})), & T_{\text{off}} \leq t < T_{\text{off}} + 3\tau \\ f_0 + +\alpha(1 - exp(-3)) - (\alpha - \beta)(1 - exp(-\frac{t-T_{\text{off}}-3\tau}{\tau_2})) & t \geq T_{\text{off}} + 3\tau \end{cases}$$

where f_0 is the signal base line, T_{off} is the starting time of the fusion process, τ and τ_2 are the fast and slow relaxation times, and α and β are the plateau values of the fast and slow relaxation regimes, respectively.
Note that the fusion signal could not be well described as a single exponential relaxation process, which was sufficient for other protein liquids studied with the same method (Patel et al., 2015; Saha et al., 2016). This suggests the onset of inertial effects, a transition often challenging to study in more conventional liquids (Eggers et al., 1999).
Plotting the time constant, τ, for the fast initial relaxation process against the characteristic length scale of the droplets (geometric radius, $r = \sqrt{(r1 * r2)}$) we estimate the ratio of dynamic viscosity to surface tension to be 13 ± 2 ms / µm (magenta fit ± 95% confidence interval in left inlet of Fig. 1C).

Surface wetting, fusion and fission of droplets

A shear flow was generated by pressing one side of a flow channel generated with silicone grease and two parallel double-sided tape in between a coverslip and a glass slide. Images were acquired using an upright spinning microscope (Leica, DM6000 B) with spinning disk head (Perkin Elmer) using a 63x glycerol-immersion objective (UPlanSApochromat, NA 1.3).

Fluorescence Recovery After Photo-bleaching (FRAP)

FRAP was performed as previously described (Brangwynne et al., 2009) in a spinning disk confocal imaging system (inverted Olympus microscope with a Yokogawa CSU-X1 scan head) fitted with diode-pumped solid-state lasers [488 nm Coherent Sapphire (50mW) and 561 nm Cobolt Jive (50mW)] using a 100x objective (UPlanSApochromat 100x NA 1.4 oil-immersion) and Andor iXon DU-897 BV back illuminated EMCCD camera. A single confocal plane was imaged over time for all FRAP experiments. A roi of ~1,07 μm^2 was photo-bleached. Image were acquired every 100 milliseconds. 30 and 1000 images were recorder before and after photo-bleaching, respectively.

Sample preparation for imaging

Drops and bundles were imaged within costum-made image chambers generated by cutting a square window in the middles of a double-sided tape (~150 µm thick). Parafilm (Cat# PM996) was used attached to the double-sided tape to cut the window. Double-sided tape still attached to the parafilm was stick to a glass slide and sealed with a microscope coverslip after removing the parafilm on top of it and adding 5 or 10 µl of sample. For conditions where reagents were added during imaging or just prior to imaging, MatTek-glass bottom dishes were used. In these cases, to avoid evaporation mineral oil (Cat# 330779, Sigma) was added on top of the sample. In all experiments oxigen scavanger mix was added to the assay buffer at the following concentrations; 40 mM D-Glucose (Cat# G7528, Sigma), 56 µg/ml, Glucose oxidase (Aspergillus niger, Cat# 22778, SERVA electrophoresis GmBH), and 11 µg/ml Catalase (Cat# C40, Sigma).

Interaction of tau drops with pre-existing microtubules (guidance) and TIRF imaging

Drops interaction with single stable microtubules (FIG. 3D) were imaged with TIRF microscopy. Microtubules and flow chambers for these experiments were prepared as described previously (Fink et al., 2009). In brief, double stabilized rhodamine-labelled microtubules templates (GMPCPP and 10 mM paclitaxel, 1x BRB80, pH 6.9) were injected into a flow chamber and bound to surface-immobilized tubulin anti-bodies. After rinsing the chamber with assay buffer (25 mM HEPES, 10 mM DTT, 0.5 mg/ml casein, 10 mM paclitaxel, 0.1% Tween, 40 mM D-glucose, 110 µg/ml glucose oxidase, and 20 µg/ml catalase), tau drops with overall concentration of 5 µM Cy5-labelled tubulin dimers were flushed into the channel. Drops were formed in the presence of 10% dextran as mentioned before. Microtubules and tau-EGFP molecules were visualized using an inverted fluorescence microscope (Axio Observer Z3, Carl Zeiss) with a Zeiss 63x oil immersion 1.46 NA TIRF objective and a build-in 1.6x optovar in combination with an Andor iXon 897 (Andor Technology) EMCCD camera controlled by Metamorph (Molecular Devices Corporation). A Lumen 200 metal arc lamp (Prior Scientific Instruments) for excitation in epi-fluorescence mode and a 488 nm, 50 mW, diode solid-state laser (Vortran) for TIRF-illumination in combination with GFP and TRITC filters (Chroma Technology) were used.

Image Analysis

Estimation of concentration of tubulin in drops

Mean fluorescent intensity of rhodamine-tubulin was measured from an image z-stack at a final total concentration of 1 µM tubulin for each condition. The mean intensity in any of the conditions without drops (see fig. S3B) was comparable to the one in the bulk medium in conditions were drops were present. To estimate the concentration of tubulin in the drops we assumed that the relation between intensity and concentration was linear and compared the intensity in the drop to the mean intensity in the conditions with tubulin alone. At 20 minutes after formation the concentration was estimated to be ~ 25 µM.

Concentration in drops in a homogeneous solution

We estimated that at an overall concentration of 5 µM of rhodamine-tubulin added to tau drops, the tubulin concentration inside the drop was 10 time higher than outside the drop (see figure 2B and S3A,C). For tau, we estimated to be enriched 7 folds in the drop compared to the bulk solution. As the volume occupied by the drops compared to that occupied by the bulk solution is around 1%, we estimated that the concentration in the bulk solution is similar to the overall concentration added. Therefore at 5 µM and 25 µM of overall concentration of tau and tubulin, we estimated to have around 50 µM of tubulin and 175 µM of tau.

Table S1

Construct	Sequence (aa)	Notes
htau441-mEGFP-PS-6xhis*	MAAAAEPRQEFEVMEDHAGTYGLGDRKDQGGYTMHQ DQEGDTDAGLKESPLQTPTEDGSEEPGSETSDAKSTPTAE DVTAPLVDEGAPGKQAAAQPHTEIPEGTTAEEAGIGDTPS LEDEAAGHVTQARMVSKSKDGTGSDDKKAKGADGKTK IATPRGAAPPGQKGQANATRIPAKTPPAPKTPPSSGEPPKS GDRSGYSSPGSPGTPGSRSRTPSLPTPPTREPKKVAVVRTP PKSPSSAKSRLQTAPVPMPDLKNVKSKIGSTENLKHQPG GGKVQIINKKLDLSNVQSKCGSKDNIKHVPGGGSVQIVY KPVDLSKVTSKCGSLGNIHHKPGGGQVEVKSEKLDFKDR VQSKIGSLDNITHVPGGGNKKIETHKLTFRENAKAKTDH GAEIVYKSPVVSGDTSPRHLSNVSSTGSIDMVDSPQLATL ADEVSASLAKQGLGAPGSAGSAAGSGMVSKGEELFTGV VPILVELDGDVNGHKFSVSGEGEGDATYGKLTLKFICTT GKLPVPWPTLVTTLTYGVQCFSRYPDHMKQHDFFKSAM PEGYVQERTIFFKDDGNYKTRAEVKFEGDTLVNRIELKGI DFKEDGNILGHKLEYNYNSHNVYIMADKQKNGIKVNFKI RHNIEDGSVQLADHYQQNTPIGDGPVLLPDNHYLSTQSK LSKDPNEKRDHMVLLEFVTAAGITLGMDELYKLEVLFQ GPGSSHHHHHHSG	Human tau cloned by PCR from tau/pET29b. Highlighted fragment was removed by 3C HRV protease.
htau441-PS-6xhis*	MAAAAEPRQEFEVMEDHAGTYGLGDRKDQGGYTMHQ DQEGDTDAGLKESPLQTPTEDGSEEPGSETSDAKSTPTAE DVTAPLVDEGAPGKQAAAQPHTEIPEGTTAEEAGIGDTPS LEDEAAGHVTQARMVSKSKDGTGSDDKKAKGADGKTK IATPRGAAPPGQKGQANATRIPAKTPPAPKTPPSSGEPPKS	Human tau cloned from hTau441-mEGFP-PS-6xhis by Not1, Asc1

	GDRSGYSSPGSPGTPGSRSRTPSLPTPPTREPKKVAVVRTP PKSPSSAKSRLQTAPVPMPDLKNVKSKIGSTENLKHQPG GGKVQIINKKLDLSNVQSKCGSKDNIKHVPGGGSVQIVY KPVDLSKVTSKCGSLGNIHHKPGGGQVEVKSEKLDFKDR VQSKIGSLDNITHVPGGGNKKIETHKLTFRENAKAKTDH GAEIVYKSPVVSGDTSPRHLSNVSSTGSIDMVDSPQLATL ADEVSASLAKQGLGAPLEVLFQGPGSSHHHHHHSG	digestion. Highlighted fragment was removed by 3C HRV protease.
htau441-mCherry-PS-6xhis*	MAAAAEPRQEFEVMEDHAGTYGLGDRKDQGGYTMHQ DQEGDTDAGLKESPLQTPTEDGSEEPGSETSDAKSTPTAE DVTAPLVDEGAPGKQAAAQPHTEIPEGTTAEEAGIGDTPS LEDEAAGHVTQARMVSKSKDGTGSDDKKAKGADGKTK IATPRGAAPPGQKGQANATRIPAKTPPAPKTPPSSGEPPKS GDRSGYSSPGSPGTPGSRSRTPSLPTPPTREPKKVAVVRTP PKSPSSAKSRLQTAPVPMPDLKNVKSKIGSTENLKHQPG GGKVQIINKKLDLSNVQSKCGSKDNIKHVPGGGSVQIVY KPVDLSKVTSKCGSLGNIHHKPGGGQVEVKSEKLDFKDR VQSKIGSLDNITHVPGGGNKKIETHKLTFRENAKAKTDH GAEIVYKSPVVSGDTSPRHLSNVSSTGSIDMVDSPQLATL ADEVSASLAKQGLGAPGSAGSAAGSGMVSKGEEDNMAI IKEFMRFKVHMEGSVNGHEFEIEGEGEGRPYEGTQTAKL KVTKGGPLPFAWDILSPQFMYGSKAYVKHPADIPDYLKL SFPEGFKWERVMNFEDGGVVTVTQDSSLQDGEFIYKVKL RGTNFPSDGPVMQKKTMGWEASSERMYPEDGALKGEIK QRLKLKDGGHYDAEVKTTYKAKKPVQLPGAYNVNIKLD ITSHNEDYTIVEQYERAEGRHSTGGMDELYKLEVLFQGP GSSHHHHHHSG	Human tau cloned from hTau441-mEGFP-PS-6xhis by Not1, Asc1 digestion. Highlighted fragment was removed by 3C HRV protease.
6xhis-PS-EGFP-htau441*	MGSSHHHHHHSSGRLEVLFQGPMVSKGEELFTGVVPILV ELDGDVNGHKFSVSGEGEGDATYGKLTLKFICTTGKLPV PWPTLVTTLTYGVQCFSRYPDHMKQHDFFKSAMPEGYV QERTIFFKDDGNYKTRAEVKFEGDTLVNRIELKGIDFKED GNILGHKLEYNYNSHNVYIMADKQKNGIKVNFKIRHNIE DGSVQLADHYQQNTPIGDGPVLLPDNHYLSTQSKLSKDP NEKRDHMVLLEFVTAAGITLGMDELYKGSAGSAAGSGA AAAEPRQEFEVMEDHAGTYGLGDRKDQGGYTMHQDQE GDTDAGLKESPLQTPTEDGSEEPGSETSDAKSTPTAEDVT APLVDEGAPGKQAAAQPHTEIPEGTTAEEAGIGDTPSLED EAAGHVTQARMVSKSKDGTGSDDKKAKGADGKTKIAT PRGAAPPGQKGQANATRIPAKTPPAPKTPPSSGEPPKSGD RSGYSSPGSPGTPGSRSRTPSLPTPPTREPKKVAVVRTPPK SPSSAKSRLQTAPVPMPDLKNVKSKIGSTENLKHQPGGG KVQIINKKLDLSNVQSKCGSKDNIKHVPGGGSVQIVYKP VDLSKVTSKCGSLGNIHHKPGGGQVEVKSEKLDFKDRV QSKIGSLDNITHVPGGGNKKIETHKLTFRENAKAKTDHG AEIVYKSPVVSGDTSPRHLSNVSSTGSIDMVDSPQLATLA DEVSASLAKQGLGAP	Human tau cloned from hTau441-mEGFP-PS-6xhis by Not1, Asc1 digestion. Highlighted fragment was removed by 3C HRV protease.
Primers	**Sequence**	**Notes**
htau441_pOCC_FW_Not1	AATAATAACATGCGGCCGCAGCTGAGCCCCGCCAGGA	Forward primer used for PCR to clone htau 441 from pET29b to pOCC vectors for Baculovirus expression. **

htau441_pOCC_R_Asc1	AATAATAACATGGCGCGCCCAAACCCTGCTTGGCCAG G	Reverse primer used for PCR from pET29b to pOCC1 vectors for Baculovirus expression.**

* All vectors in pOCC series contain a flexible linker between the protein of interest and the adjacent tag.

**pOCC series of vectors already include an ATG and stop codon in frame with Not1 and Asc1 restriction enzymes of the PCR product (flanking arms). Hanging arms of primers are shown in red.

Supplemental Figures

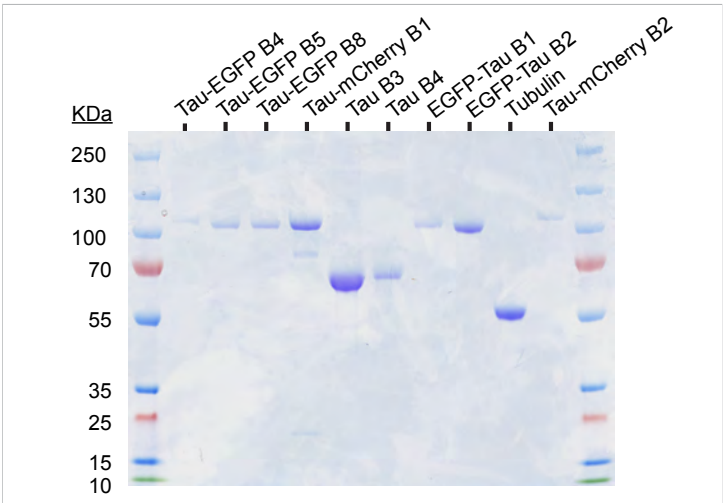

Figure S1. Recombinant proteins used in this study

(A) SDS-PAGE of the purified proteins used in this study (stained with Coomassie blue). B refers to protein batch number.

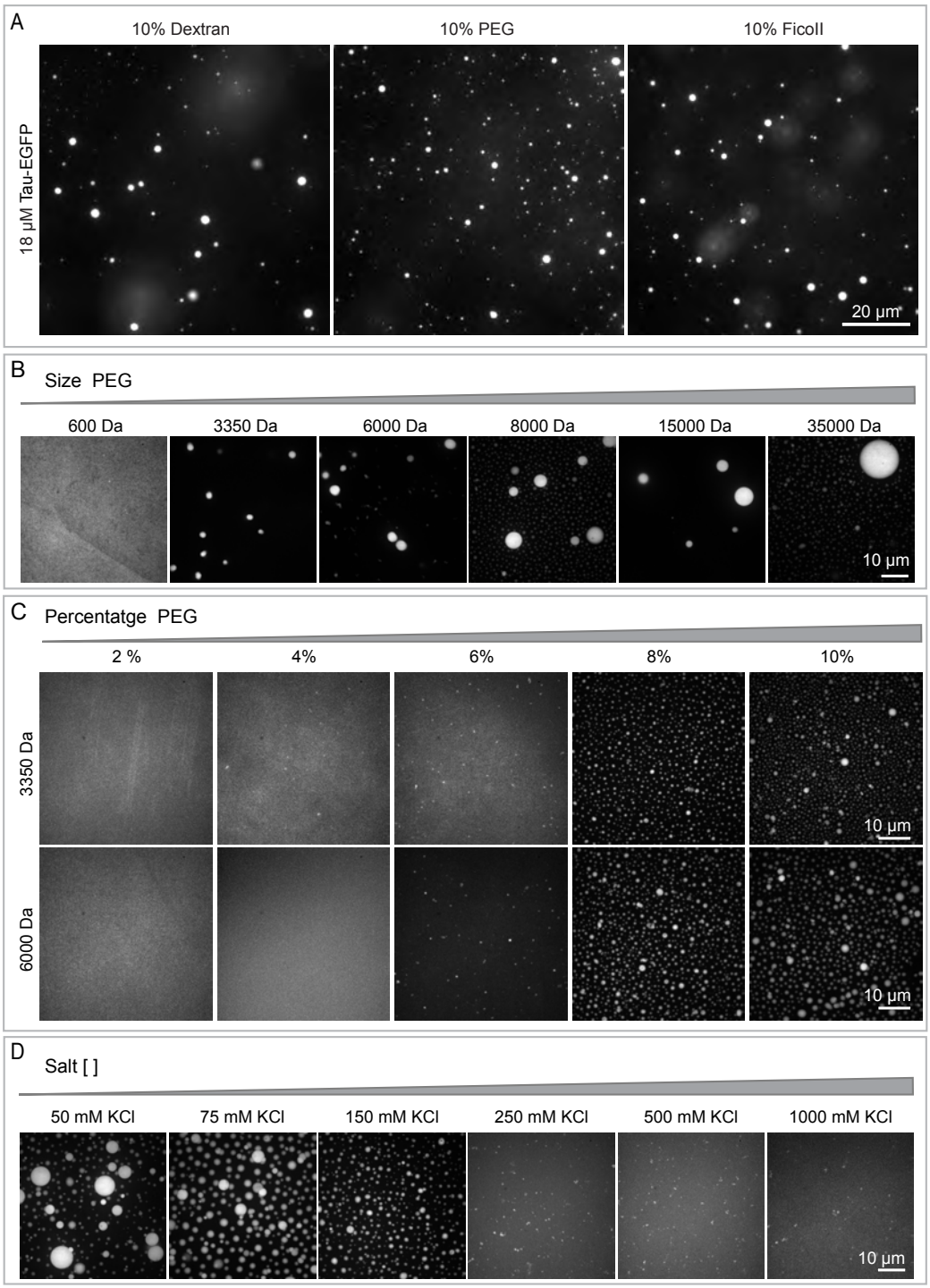

Figure S2. Tau drops are sensitive to the size and percentage of the molecular crowder and the concentration of salt

(A) *In vitro* formation of tau drops in the presence of different crowding agents. Tau drops are observed in dextran, PEG and Ficoll. Tau drops were formed with 18 µM of tau-EGFP, 25 mM HEPES, 150 mM KCl, 1 mM DTT, pH 7.4, in the presence of 10% of the indicated crowding agents; dextran (T500), PEG-8000 (Polyethylene glycol of 8000 daltons) or Ficoll-400. **(B)** Tau drops sensitivity to the size of the molecular crowder. Tau drops formation with 10% PEG of different sizes. Using 10% PEG, drops were observed at PEG sizes equal or bigger than 3350 daltons. **(C)** Tau drops sensitivity to the percentage of the molecular crowder. Tau drops formation were observed above 6% PEG for PEG sizes of 3350 and 6000 daltons. For B and C drops were formed with 25 µM of tau 1/10 labelled with EGFP, 25 mM HEPES, 150 mM KCl, 1 mM DTT, pH 7.4 in the presence of the indicated PEG and percentage. **(D)** Tau sensitivity to salt concentration. Low salt enhances drop formation while high salt inhibits it. Tau drops formation in 25 mM HEPES at the concentrations of salt indicated, pH 7.4. Tau drops were formed with 25 µM of tau-EGFP.

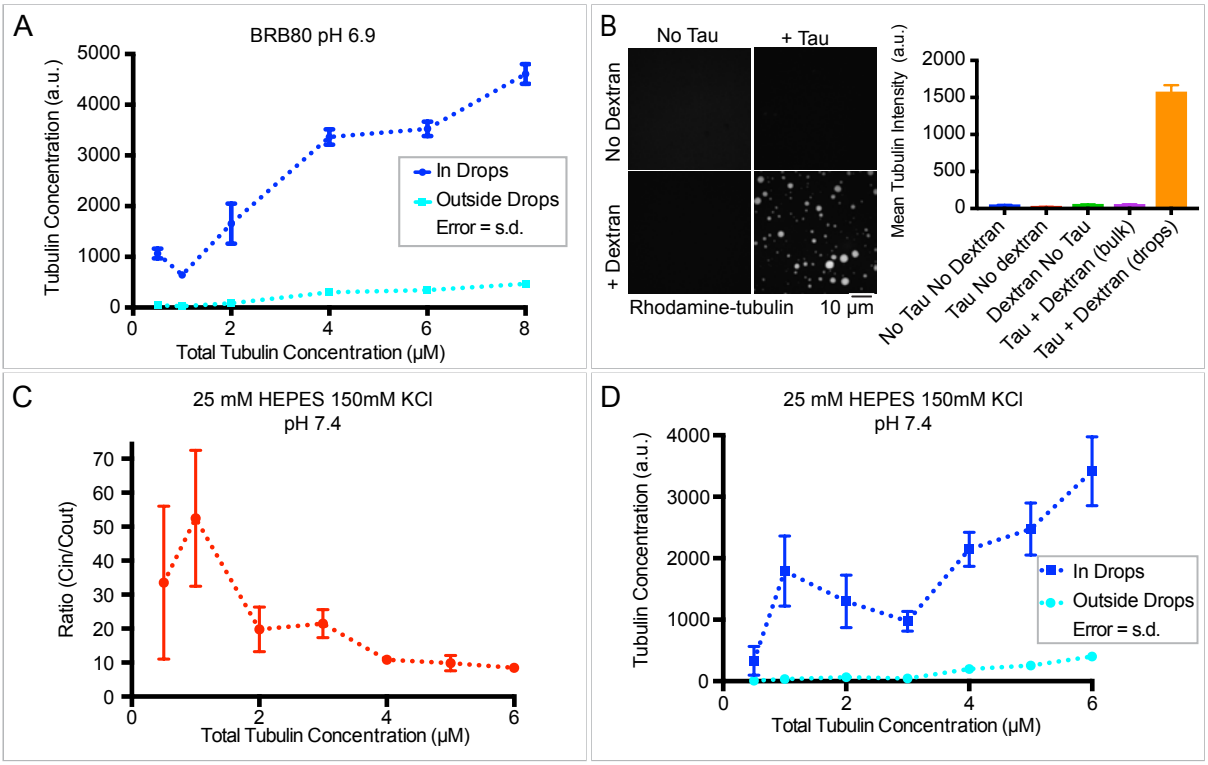

Figure S3. Tubulin partition into tau drops

(A) Tubulin concentration inside tau drops (dark blue) and in the surrounding bulk media (pale blue) quantified by mean intensity at different concentrations of total levels of tubulin (in absence of GTP) in BRB80 buffer. Values shown are the mean ± SD, n=16 image stacks were analysed, 50 images per stack. **(B)** Estimation of tubulin concentration in drops. Mean intensity of rhodamine-labelled tubulin at 1 μM of overall tubulin in conditions without drops (tubulin or tubulin plus dextran or tau) or in the presence of drops (tau plus dextran and tubulin). Proteins were dissolved in 1x BRB80, with 1 mM DTT and 10% dextran or 25 μM of tau when indicated. Assuming a linear relation between intensity and concentration for fluorescently-labelled tubulin, the estimated tubulin concentration in the drops is higher than 20 μM, 20 min after the addition of 1 μM of overall concentration of tubulin at room temperature (see M&M for details in the estimation). All experiments were carried out at room temperature. **(C)** Tubulin enrichment in drops using 25mM HEPES, 150 mM KCl, pH7.4 as buffer. Enrichment in drops was calculated by the ratio of the mean intensity inside the drops (dark blue in D) to the mean intensity in the surrounding bulk media (pale blue in D) at different concentrations of overall tubulin (no GTP added). Values shown are the mean ± SD, n=16 image stacks, 50 images per stack, mean of all drops in the stack. **(D)** Tubulin concentration inside tau drops (dark blue) and in the surrounding bulk media (pale blue) quantified as in A but for drops formed in 25 mM HEPES, 150 mM KCl, pH7.4.

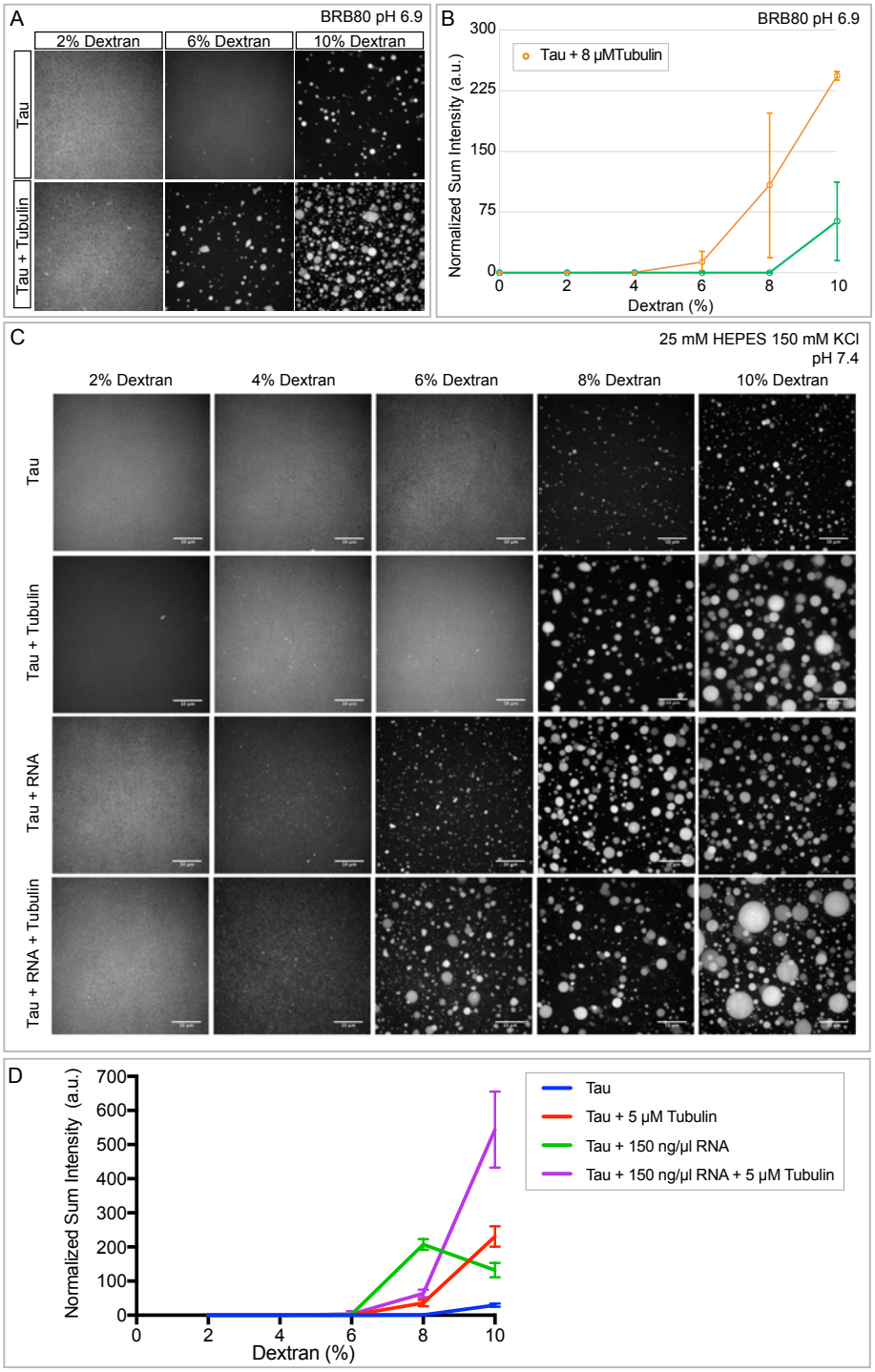

Figure S4. Tubulin and RNA enhance tau drops nucleation

(A) Representative images of tau drops' formation at different concentrations of dextran in the presence or absence of 8 µM unlabelled tubulin (in absence of GTP). **(B)** Normalized sum intensity (sum of intensity in all drops detected in a z-stack) at different concentration of dextran and in the presence or absence of 8 µM unlabelled tubulin (in absence of GTP). Values shown are the mean ± SD, N=3, 16 image stacks of 50 images per stack were analysed for each biological replica. Drops were formed with 25 µM of tau-EGFP in 1x BRB80 with the amount of dextran indicated and 1 mM DTT. **(C)** Representative images of tau drops' formation at different concentrations of dextran in the presence or absence of 150 ng/µl of RNA (total RNA) and/or 5 µM of unlabelled tubulin (in absence of GTP). Drops were formed in 25 mM HEPES, 150 mM KCl, pH 7.4 with 25 µM of Tau-EGFP and the amount of crowding indicated. Similar to tubulin, RNA enhanced tau drop formation. **(D)** Normalized sum intensity (sum of intensity in all drops detected in a z-stack) at different concentration of dextran for the conditions shown in the panel above. Values shown are the mean ± SD of 16 images stacks, 50 images per stack were analysed.

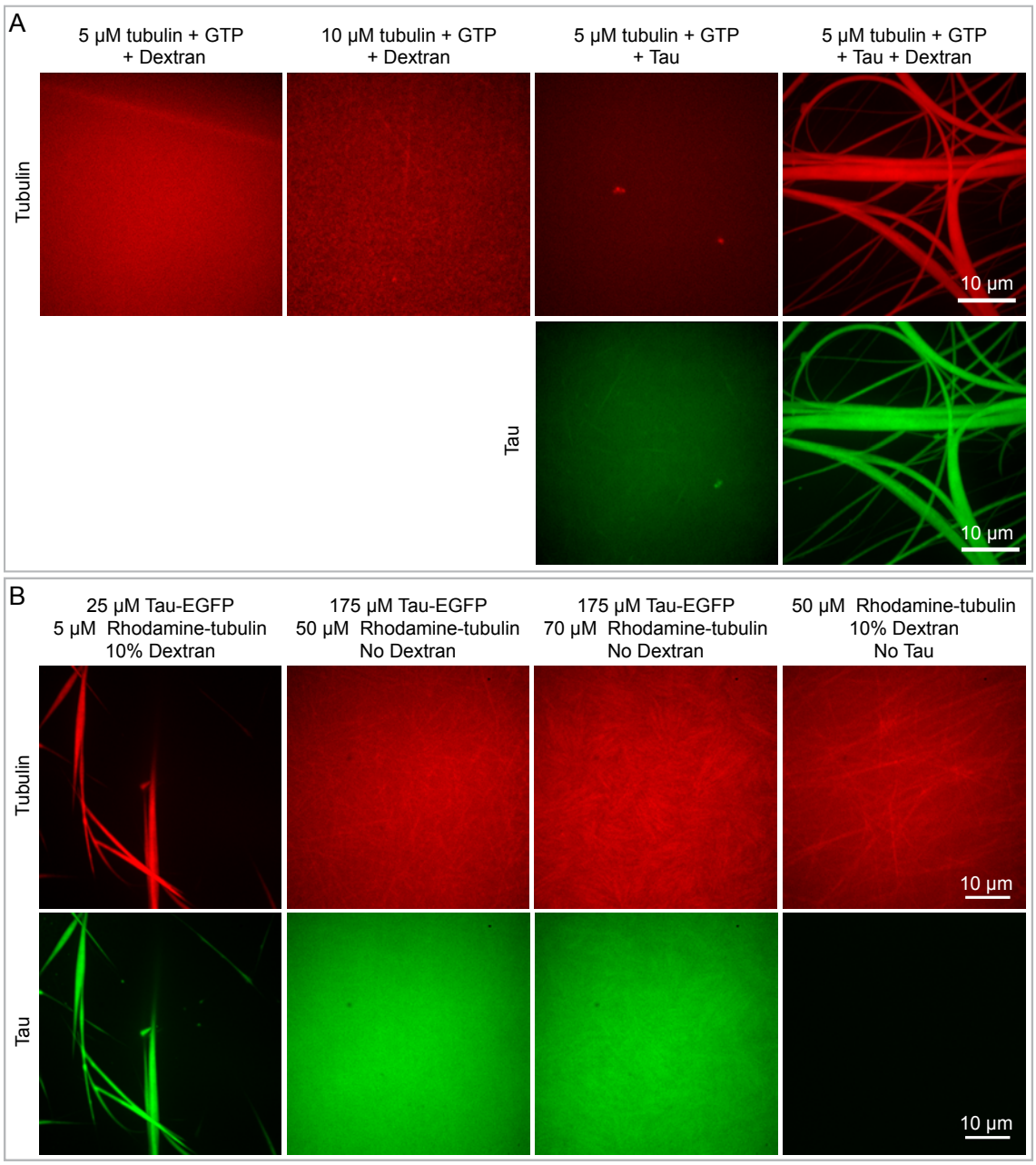

Figure S5. Tau drops are needed for tubulin concentration and bundles polymerization

(A) Upper panel, rhodamine-tubulin. Lower panel, tau-EGFP. Neither, 5 or 10 µM of tubulin in the presence of 10% dextran (room temperature) is sufficient to polymerize microtubules (first and second row). 5 µM of tubulin in the presence of tau (no dextran, no drops, room temperature) allows the polymerization of single small microtubules (third row). See also movie 6. In the presence of drops (tau plus dextran), 5 µM tubulin is sufficient for the polymerization of long tau-encapsulated bundles of microtubules. 25 µM of tau-EGFP in 1x BRB80 with the indicated amount of rhodamine-tubulin and 1 mM GTP plus 1 mM DTT were used. As mentioned, all experiments were carried out at room temperature. **(B)** Microtubules polymerization using the concentrations of tau and tubulin estimated to be in the drops in the absence of drops (no dextran or no tau). We estimated that the concentration of tau and tubulin in the drop is 7 and 10-fold enriched respectively compared to the bulk solution at this particular concentration of tau and tubulin; that is, 175 µM of tau (7 x 25 µM) and 50 µM of tubulin (10 x 5 µM). Upper panel, rhodamine-tubulin. Lower panel, tau-EGFP. First row, control situation, in the presence of drops (25 µM of tau-EGFP with 5 µM of rhodamine-tubulin and 10% Dextran in 1x BRB80 with 2 mM GTP and 1 mM DTT). Row 2 and 3, 175 µM of tau and 50 µM or 70 µM of tubulin respectively in the absence of dextran (no drops). Small microtubules are present but they do not bundle. Row 4, microtubules polymerization at 50 µM of tubulin in the presence of dextran but without tau. Neither in this case thick microtubules bundles are observed.

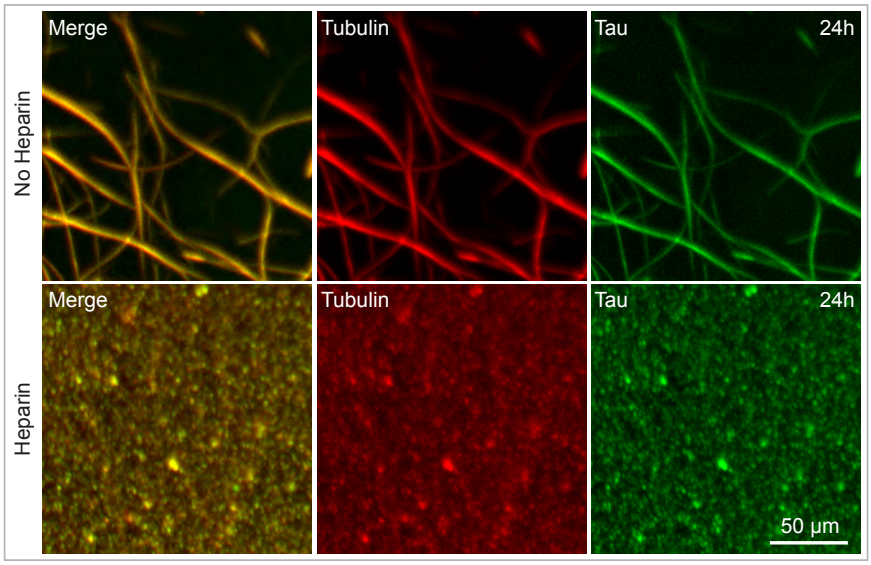

Figure S6. Tau-encapsulation stabilizes microtubules. Tau-encapsulated microtubule bundles with or without heparin observed 24 hours after formation. Bundles were formed from tau drops by addition of 5 µM rhodamine-tubulin and 1 mM GTP. Drops were formed with 25 µM of tau-EGFP in 1x BRB80 with 10% dextran and 1 mM DTT. Heparin was added at 200 µg/ml (final concentration) 30 minutes after bundles formation as indicated. Samples were incubated at room temperature for the duration of the experiment. Maximum projection confocal images are shown.

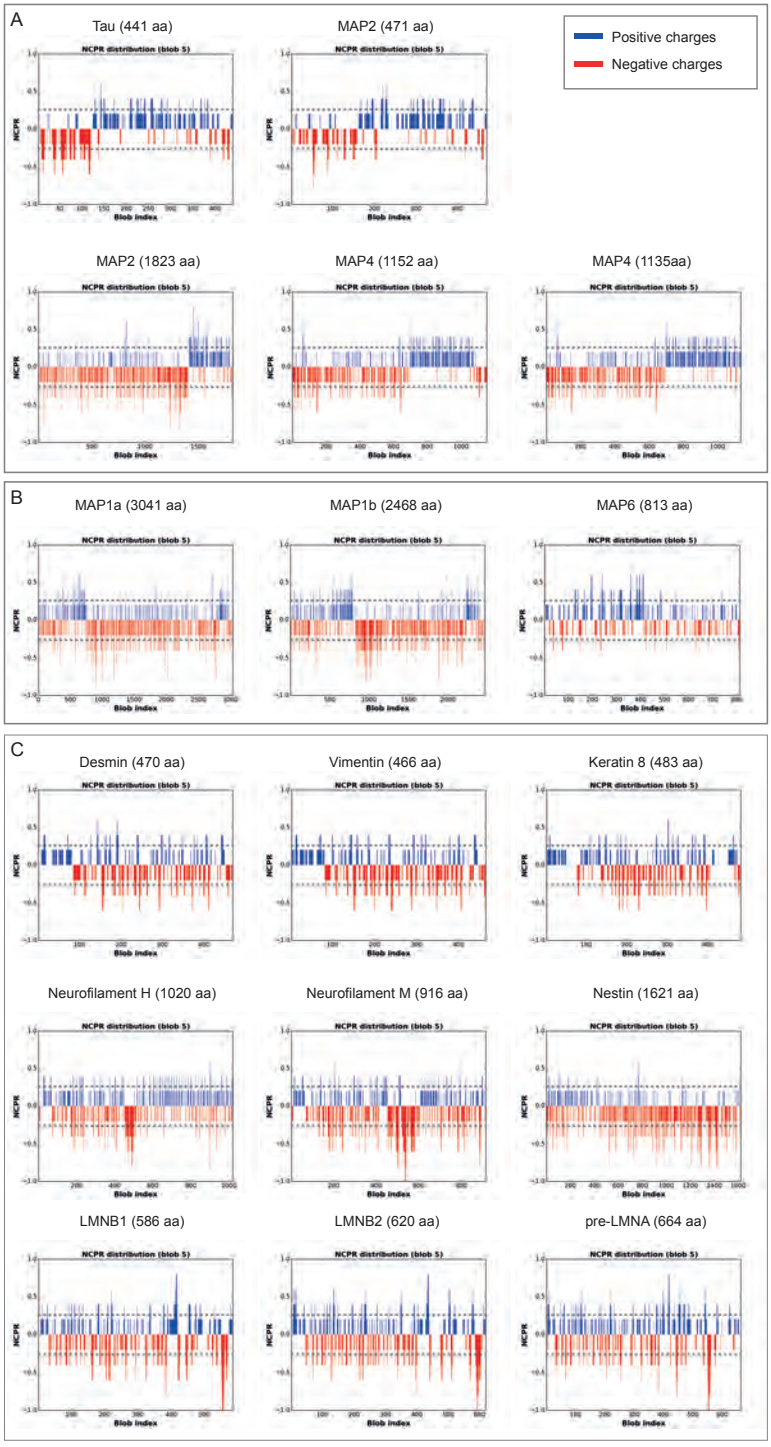

Figure S7. Charge distribution along MAPs and other cytoskeleton proteins

Charge distribution along different proteins obtained using CIDER (Classification of Intrinsically Disordered Ensemble). The net charge per residue (NCPR) is plotted with blue and red showing positive and negatively charged blocks, respectively. **(A)** Charge distribution for tau and its paralogues genes MAP2 and MAP4. The charge distribution for two different isoforms of MAP2 and MAP4 are plotted. A similar distribution of opposite charges blocks is observed for tau, MAP2 and 4, with the N-terminal part of the protein having a net negatively charged, the middle part being mainly positively charged and a small block of negative charged residues in the C-terminal end present in some cases. **(B)** Charge distribution for other MAPs. MAP1a and MAP1b show a mainly negative region in the middle part of the protein with small regions of opposite charges in the N-terminal part. The charge distribution for MAP6 shows less defined regions with opposite charges. **(C)** Charge distribution for different intermediate filament proteins. Most of them show a clear positive block of residues in the N-terminal part of the protein being less define or similar in the middle or C-terminal part of the protein.

Supplemental References

Brangwynne, C.P., Eckmann, C.R., Courson, D.S., Rybarska, A., Hoege, C., Gharakhani, J., Jülicher, F., and Hyman, A.A. (2009). Germline P granules are liquid droplets that localize by controlled dissolution/condensation. Science *324*, 1729-1732.

Eggers, J., Lister, J.R., and Stone, H.A. (1999). Coalescence of liquid drops. Journal of Fluid Mechanics *401*, 293-310.

Fink, G., Hajdo, L., Skowronek, K.J., Reuther, C., Kasprzak, A.A., and Diez, S. (2009). The mitotic kinesin-14 Ncd drives directional microtubule–microtubule sliding. Nature cell biology *11*, 717-723.

Gell, C., Friel, C.T., Borgonovo, B., Drechsel, D.N., Hyman, A.A., and Howard, J. (2011). Purification of tubulin from porcine brain. Microtubule Dynamics: Methods and Protocols, 15-28.

Hedgepeth, C.M., Conrad, L.J., Zhang, J., Huang, H.-C., Lee, V.M., and Klein, P.S. (1997). Activation of the Wnt signaling pathway: a molecular mechanism for lithium action. Developmental biology *185*, 82-91.

Holehouse, A.S., Ahad, J., Das, R.K., and Pappu, R.V. (2015). CIDER: Classification of Intrinsically Disordered Ensemble Regions. Biophysical Journal *108*, 228a.

Hyman, A., Drechsel, D., Kellogg, D., Salser, S., Sawin, K., Steffen, P., Wordeman, L., and Mitchison, T. (1991). [39] Preparation of modified tubulins. Methods in enzymology *196*, 478-485.

Jahnel, M., Behrndt, M., Jannasch, A., Schäffer, E., and Grill, S.W. (2011). Measuring the complete force field of an optical trap. Optics letters *36*, 1260-1262.

Obradovic, Z., Peng, K., Vucetic, S., Radivojac, P., Brown, C.J., and Dunker, A.K. (2003). Predicting intrinsic disorder from amino acid sequence. Proteins: Structure, Function, and Bioinformatics *53*, 566-572.

Patel, A., Lee, H.O., Jawerth, L., Maharana, S., Jahnel, M., Hein, M.Y., Stoynov, S., Mahamid, J., Saha, S., Franzmann, T.M*., et al.* (2015). A Liquid-to-Solid Phase Transition of the ALS Protein FUS Accelerated by Disease Mutation. Cell *162*, 1066-1077.

Saha, S., Weber, C.A., Nousch, M., Adame-Arana, O., Hoege, C., Hein, M.Y., Osborne-Nishimura, E., Mahamid, J., Jahnel, M., and Jawerth, L. (2016). Polar positioning of phase-separated liquid compartments in cells regulated by an mRNA competition mechanism. Cell *166*, 1572-1584. e1516.

Woodruff, J.B., and Hyman, A.A. (2015). Method: in vitro analysis of pericentriolar material assembly. Methods in cell biology *129*, 369-382.

Wootton, J.C. (1994). Non-globular domains in protein sequences: automated segmentation using complexity measures. Computers & chemistry *18*, 269-285.

Xue, B., Dunbrack, R.L., Williams, R.W., Dunker, A.K., and Uversky, V.N. (2010). PONDR-FIT: a meta-predictor of intrinsically disordered amino acids. Biochimica et Biophysica Acta (BBA)-Proteins and Proteomics *1804*, 996-1010.